A Dugdale model based geometrical amplifier enables the measurement of separation-to-failure for a cohesive interface

Yu-Jie Wei[a)]
State Key Laboratory of Nonlinear Mechanics, Institute of Mechanics, Chinese Academy of Sciences, Beijing 100190, China

(Received 17 October 2010; accepted 28 November 2010; published online 10 January 2011)

Abstract Regardless of all kinds of different formulae used for the traction-separation relationship in cohesive zone modeling, the peak traction $\sigma_{\rm m}$ and the separation-to-failure δ_0 (or equivalently the work-to-separation Γ) are the primary parameters which control the interfacial fracture behaviors. Experimentally, it is hard to determine those quantities, especially for δ_0, which occurs in a very localized region with possibly complicated geometries by material failure. Based on the Dugdale model, we show that the separation-to-failure of an interface could be amplified by a factor of $L/r_{\rm p}$ in a typical peeling test, where L is the beam length and $r_{\rm p}$ is the cohesive zone size. Such an amplifier makes δ_0 feasible to be probed quantitatively from a simple peeling test. The method proposed here may be of importance to understanding interfacial fractures of layered structures, or in some nanoscale mechanical phenomena such as delamination of thin films and coatings. © *2011 The Chinese Society of Theoretical and Applied Mechanics.* [doi:10.1063/2.1101106]

Keywords cohesive zone, dugdale model, separation-to-failure, thin film, peeling test

Started with the work of Barenblatt[1] and Dugdale,[2] cohesive interface modelling of fractures has a history of half century. In recent years, cohesive surface models have been widely used to numerically simulate fracture initiation and growth by the finite-element method; [3–5] for recent reviews see Refs. [6,7]. An important characteristic of this methodology for modelling fracture initiation and crack propagation is that macroscopic fracture criteria based on elastic or elastic-plastic analyses, such as $K_{\rm IC}$ or $J_{\rm IC}$, is characterized by the local traction-separation relation and the cohesive surface methodology. Propagation of cracks along potential paths will be automatically determined by local deformation status.

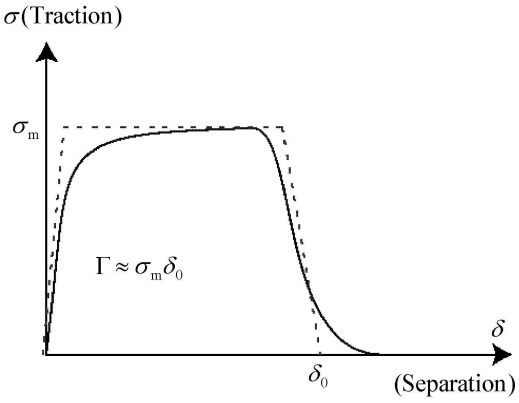

Fig. 1. A typical traction (σ) and separation (δ) relationship (solid curve) and its corresponding trapezoidal representation (dotted lines). It is noted that the work-to-separation Γ is given as $\Gamma = \sigma_{\rm m}\delta_0$.

a)Corresponding author. E-mail: yujie_wei@lnm.imech.ac.cn.

Different formats of traction-separation laws have been suggested, including the non-linear reversible elastic type,[4,8] triangular or trapezoidal model,[9–14] Viscous-regulated cohesive model,[15–17] Non-elastic, plastic softening modeling,[5,18] and reversible elastic-irreversible plastic model.[19–21] Their applications range from grain-boundary failure in crystalline materials, delamination in composite materials, to the debonding of adhesive joints. Regardless of all kinds of different formulae used for the traction-separation relationship in cohesive zone modeling, the peak traction $\sigma_{\rm m}$ and the separation-to-failure δ_0, or equivalently the work-to-separation Γ, are the primary parameters which control the interfacial fracture behaviors.[9,10] The details of traction-separation plays a second role; Fig. 1 shows such a typical traction-separation law, where the equivalence between δ_0 and Γ is also seen. Mechanically, it is desired to obtain those two critical parameters in an interface during relatively simple calibrating tests so that the properties can be used in simulations to capture the mechanical response of more complex loading and/or geometrical conditions. Several experimental techniques have been used to characterize the interfacial toughness Γ[22] but no experiments are available for δ_0. The difficulty to obtain δ_0 through experiments is evident: (a) interfacial failure usually occurs in a very localized region with complicated local structures due to a broken interface, and it is hard to measure any quantities there with confidence; (b) δ_0 is in general small and could be in the order of nanometers. Based on the Dugdale model and beam theories, we show that the separation-to-failure could be amplified by a factor of $L/r_{\rm p}$ in a peeling test, where L is the beam length and $r_{\rm p}$ is the typical cohesive zone size. Such an amplifier makes it feasible to probe δ_0 quantitatively from

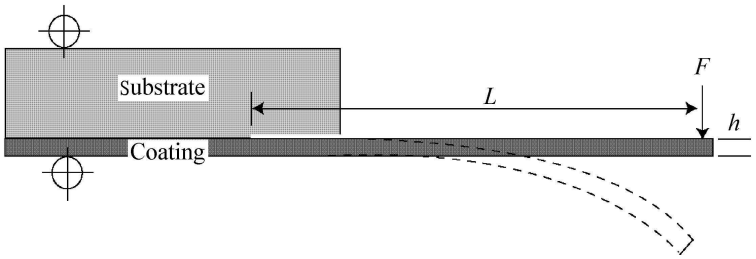

Fig. 2. The setup of a peeling test, from which the separation-to-failure for the interface can be amplified.

simple peeling tests.

We take a thin film on a substrate as a demonstration, as shown in Fig. 2. Similar structures have been used to measure the energy release rate of diamond coatings on tungsten carbide substrate.[23] For interfacial fracture, it is noted that the peak strengths ($\sigma_{\rm m}$ and $\tau_{\rm m}$) and the fracture toughness ($G_{\rm c}$) are the most important parameters.[9,10] The details of the traction-separation play a second role. Different methods have been developed to obtain the fracture toughness of an interface. One simple but effective way is to obtain the crack tip energy release rate G from the compliance of the specimen as an interfacial crack propagates, by applying the classical result

$$G = \frac{F^2}{2}\frac{\partial c}{\partial a}, \tag{1}$$

where F is the applied load, c is the compliance of the structure, and a is the crack length. The energy release rate computed in this way can be taken to be equal to the effective toughness of the material. For the configuration in Fig. 2, it is easy to show that, in the quasi-static condition, the theoretical energy release rate per unit area is

$$G = \frac{F^2}{2B}\frac{L^2}{EI}, \tag{2}$$

where B is the width of the beam, E is the Young's modulus of the coating, and I is the inertia moment of the beam. For a rectangular beam, $I{=}Bh^3/12$. The critical condition for crack propagation is $G = G_c$. With G, we could hence obtain $\sigma_{\rm m}\delta_0$ for a Dugdale cohesive zone.[24,25] Next, we show how δ_0 is amplified by the presence of the cohesive zone.

With the Dugdale cohesive zone, the deflection of a beam shown in Fig. 3(a) will be influenced via the change in boundary conditions. As seen in Fig. 3(b), there could be some deflection in the cohesive zone even though there is no apparent failure in that region. The possible traction applied to the beam in this circumstance, is given in Fig. 3(c).Now the cantilever beam may have prescribed loading and boundary conditions shown in Fig. 3(d). In this case, we express the distributed load $q(x)$ in the beam as

$$\begin{aligned} q(x) = {} & M_0\langle x\rangle^{-2} + R_0\langle x\rangle^{-1} + \sigma_{\rm m}\langle x\rangle^0 \\ & - \sigma_{\rm m}\langle x - r_{\rm p}\rangle^0 - F\langle x - L - r_{\rm p}\rangle^{-1}, \end{aligned} \tag{3}$$

where $\langle x-a\rangle$ are singularity functions. The definition of such singularity functions is following: (I)$\langle x-a\rangle^{-2} = 0$ if $x \neq a$, $\langle x-a\rangle^{-2} = \pm\infty$ at $x = a$, and $\int \langle x-a\rangle^{-2} = \langle x-a\rangle^{-1}$; (II)$\langle x-a\rangle^{-1} = 0$ if $x \neq a$, $\langle x-a\rangle^{-1} = +\infty$ at $x = a$, and $\int \langle x-a\rangle^{-1} = \langle x-a\rangle^{0}$; (III) $\langle x-a\rangle^{0} = 0$ if $x < a$, $\langle x-a\rangle^{0} = 1$ for $x \geq a$, and $\int \langle x-a\rangle^{0} = \langle x-a\rangle^{1}$; (IV) $\langle x-a\rangle^{0} = 0$ if $x < a$, $\langle x-a\rangle^{1} = x-a$ for $x \geq a$, and $\int \langle x-a\rangle^{1} = \langle x-a\rangle^{2}/2$. Integrating Eq. (3) from 0 to $L + r_{\rm p}$, we readily obtain shear force

$$\begin{aligned} V(x) = {} & M_0\langle x\rangle^{-1} + R_0\langle x\rangle^0 + \sigma_{\rm m}\langle x\rangle^1 \\ & - \sigma_{\rm m}\langle x - r_{\rm p}\rangle^1 - F\langle x - L - r_{\rm p}\rangle^0 \end{aligned} \tag{4a}$$

and moment along the beam

$$\begin{aligned} M(x) = {} & M_0\langle x\rangle^0 + R_0\langle x\rangle^1 + \sigma_{\rm m}\langle x\rangle^2/2 \\ & - \sigma_{\rm m}\langle x - r_{\rm p}\rangle^2/2 - F\langle x - L - r_{\rm p}\rangle^1. \end{aligned} \tag{4b}$$

For a location with x slightly beyond $L + r_{\rm p}$,there should be no shear force or moment. Hence it is convenient to yield the shear force

$$R_0 = F - \sigma_{\rm m} r_{\rm p} \tag{5a}$$

and the bending moment

$$M_0 = -F(L + r_{\rm p}) - \sigma_{\rm m} r_{\rm p}^2/2 \tag{5b}$$

at x=0. Relating the beam deflection to moment by

$$EI\frac{{\rm d}^2 y}{{\rm d}x^2} = M(x) \tag{6}$$

we get the beam deflection.

$$\begin{aligned} EI\, y(x) = {} & \frac{M_0\langle x\rangle^2}{2} + \frac{R_0\langle x\rangle^3}{6} + \frac{\sigma_{\rm m}\langle x\rangle^4}{24} \\ & - \frac{\sigma_{\rm m}\langle x - r_{\rm p}\rangle^4}{24} - \frac{F\langle x - L - r_{\rm p}\rangle^3}{6} + c_1 x + c_0 \end{aligned} \tag{7}$$

Applying the two boundary conditions

$$EI\, y|_{x=0} = 0 \text{ and } EI\, y|_{x=r_{\rm p}} = -\delta_0 \tag{8}$$

we obtain

$$c_0 = 0 \text{ and } c_1 = -\frac{EI\delta_0}{r_{\rm p}} - \frac{M_0 r_{\rm p}}{2} - \frac{R_0 r_{\rm p}^2}{6} + \frac{\sigma_{\rm m} r_{\rm p}^3}{24}.$$

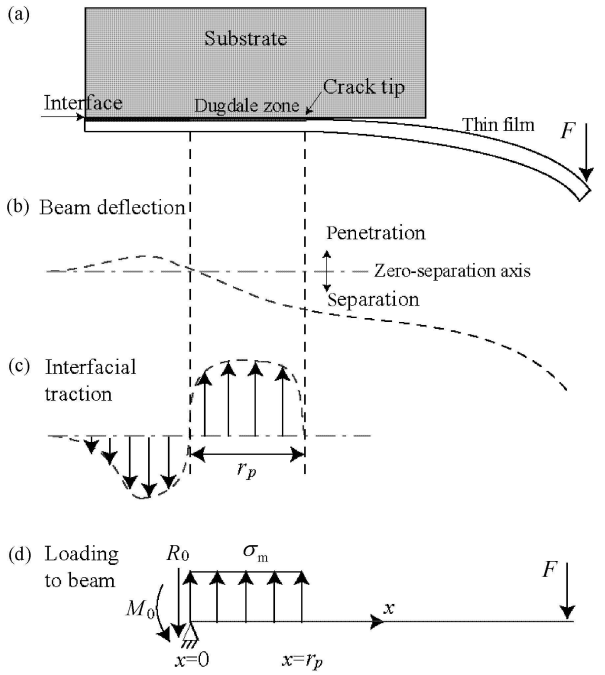

Fig. 3. The illustration to show beam deflection influenced by Dugdale cohesive zone. (a) The setup a peeling test; (b) interfacial separation/penetration (deflection of the idealized beam represented by the dashed line); (c) schematic of interfacial stress due to the separation/penetration of two surfaces; (d) constructed beam loading based on (a), (b) and (c). It is noted that the beam is assumed to be simply supported at x=0 since there is no interfacial separation/penetration there. The beam deflection at $r_{\rm p}$ is given as δ_0 — the separation-to-failure. M_0 and R_0 are the moment and shear force at x=0, which are to be determined.

Neglecting higher order terms for $r_{\rm p}$ since $L >> r_{\rm p}$, we obtain the deflection at the beam tip

$$y(L+r_{\rm p}) = -\frac{FL^3}{3EI} - \frac{L}{r_{\rm p}}\delta_0. \tag{9}$$

Here the first term is the standard part from a clamped beam, and the second term comes from the contribution by the Dugdale zone. The separation-to-failure of the interface is amplified by the factor $L/r_{\rm p}$. We note that Eq. (9) is valid only when the cohesive zone is fully developed, i.e. the crack front reaches the critical condition to fail, which is implied in the boundary condition in Eq. (8). Such an amplifier makes δ_0 feasible to be probed quantitatively from a simple peeling test. Next, we will use finite element simulation to validate the assumptions made in Fig. 3 and the load-deflection relationship given in Eq. (9).

We simulated the beam deflection problem using the geometries given in Fig. 4. Both the substrate and the film coating was assumed to deform elastically with the same Young's moduli E=200 GPa and Poisson's ratio ν=0.3. The typical element size in the simulation was about one tenth of the beam thickness, and those nearby the crack tip were about one fiftieth of the beam thickness. An abaqus [26] user interface subroutine was used to simulate the interfacial response. For the details of the model, the reader is referred to Wei and Anand.[19]

Before jumping to the simulation results, we first give an estimate about the cohesive zone size. Irwin[27] gave the relationship between the critical energy release rate and the fracture toughness as

$$G = \frac{K_{\rm IC}^2}{E/(1-v^2)} \tag{10}$$

for plane strain condition. With G=$\sigma_{\rm m}\delta_0$ and $K_{\rm IC}$ = $Q\,\sigma_{\rm m}\sqrt{\pi r_{\rm p}}$, where Q is a geometrical factor, we have an estimate for the cohesive zone size

$$r_{\rm p} = \frac{E}{\sigma_{\rm m}Q^2(1-\nu^2)\pi}\delta_0 \tag{11}$$

Since Q is unknown for the specific geometry given in Fig. 4, we will use an approximation of $r_{\rm p}$= $E\delta_0/10\sigma_{\rm m}$. It gives $r_{\rm p}$=100 and δ_0=0.2 μm from the traction-separation curve shown in Fig. 5. The load-displacement curve obtained from the peeling simulation is shown in Fig. 6. A difference between the theoretical prediction without a cohesive zone and the simulated result is clearly observed. This difference is attributed to the presence of the cohesive zone.

We have plotted the traction vs. position from the crack tip at different time sequences, see Fig. 7. The development of the cohesive zone is observed. When the element at the crack tip reaches its critical separation-to-failure, the size of the cohesive zone will remain almost constant as the crack propagates. Note that the cohesive zone size from our simulation is about one half of our estimation from Eq. (11). The difference may originate from our assumption of the geometric factor Q in the equation. If we use the cohesive zone size from the simulation shown in Fig. 7, which is about 0.1 μm, as well as the separation-to-failure used for the interface δ_0=2 nm (Fig. 5), we have $\delta_0/r_{\rm p}$=0.02. This ratio is consistent with the simulation result shown in Fig. 6, where $\delta_0/r_{\rm p}$ ≈0.015. The difference may originate from both the assumption that there is a uniform distribution of traction in the cohesive zone and our approximation to the cohesive zone size of $r_{\rm p}$=0.1 μm. The evolution of separation vs. position is shown in Fig. 8. It also confirms that the node at the crack tip reaches its separation-to-failure.

In conclusion, we have supplied an analysis which may help to measure the separation-to-failure δ_0 in a Dugdale cohesive zone. It is found that δ_0 could be amplified by a factor of $L/r_{\rm p}$ in a typical peeling test, where L is the beam length and $r_{\rm p}$ is the cohesive zone size. Finite-element simulation also validates the assumption made to derive the amplified deflection. It is expected that,approaches the second term, e.g. increasing the beam thickness or width, δ_0 could be measured with reasonable accuracy. Since deformation in adherents are assumed to be purely elastic in our analysis, Eq. (9) may be only valid in the case that the yield

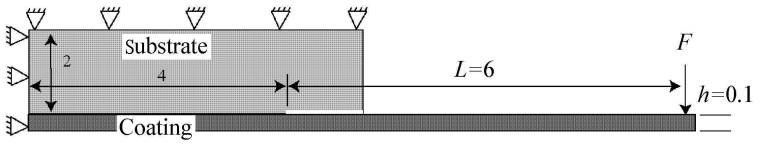

Fig. 4. The beam-substrate assembly used for finite element simulation. The unit of the dimension given above is in micrometers (m) although it could be scaled to other units in a finite-element simulation.

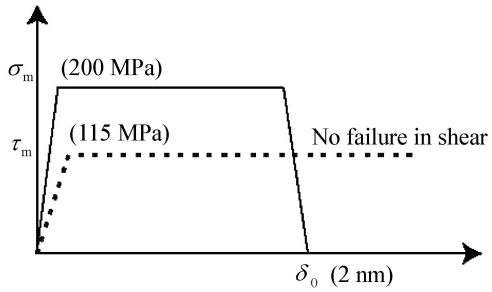

Fig. 5. The traction-separation low used for the substrate-coating interface shown in Fig. 4. The traction-separation in mode I fracture gives an interfacial toughness $\Gamma = 40\,\mathrm{mJ/m^2}$. The shear resistance to sliding is taken to be a constant $\tau_m = 114\,\mathrm{MPa}$, and the interface wouldn't be failed by shearing.

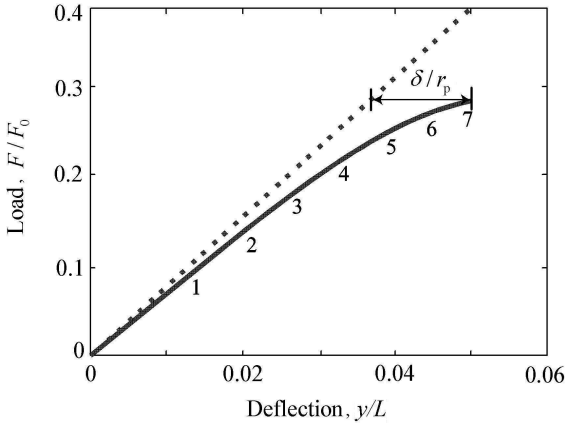

Fig. 6. Load (normalized by $F_0 = 3EI/L^2$) vs. deflection (normalized by L) for the peeling simulation. The load at the end corresponding to the critical condition where the point at the crack front starts to fail. The dotted line is for the case of no cohesive zone. The distance between the ends of the two curves is δ_0/r_p, which is contributed to by the cohesive zone.

strength of the adherents is much higher than the interfacial strength σ_m. We note that there could be cohesive laws which have a long tail, for which the cohesive energy is well defined but not the critical separation.[28,29] The theory presented here is not suitable for such types of long tail cohesive laws.

It is confirmed that the critical separation at crack tip reaches δ_0.

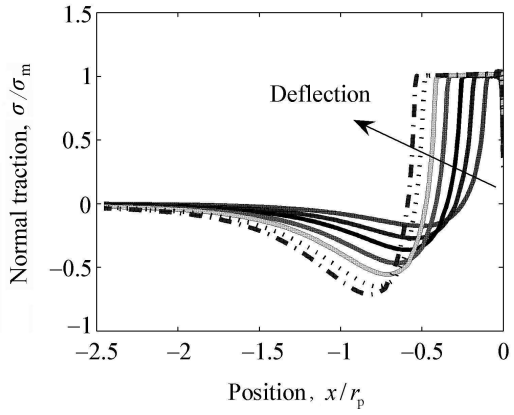

Fig. 7. Normal traction (normalized by σ_m) vs. position (x/r_p) from the crack tip (x=0) at different time sequences keyed in Fig. 6. At the last step, the cohesive zone is fully developed. There is almost no change of the size of the cohesive zone for further loading.

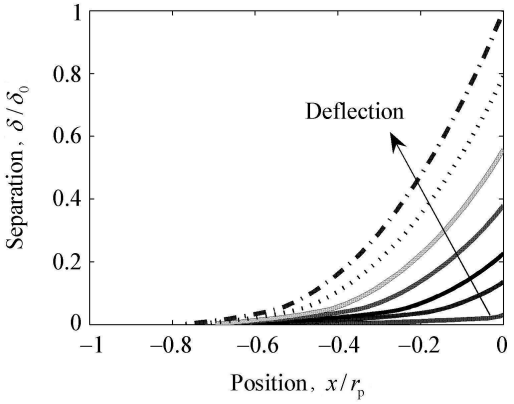

Fig. 8. Interfacial separation (normalized by δ_0) vs. position (normalized by r_p) from the crack tip (x=0) at different time sequence keyed in Fig. 6.

The work was supported by the "Hundred Talent Program" from Chinese Academy of Sciences.

1. G. I. Barenblatt, Appl. Math. Mech. (PMM) **23**, 622 (1959).
2. D. S. Dugdale, J. Mech. Phys. Solids **8**, 100 (1960).
3. A. Needleman, Int. J. Frac. **40**, 21 (1990).
4. X. P. Xu and A. Needleman, J. Mech. Phys. Solids **42**, 1397 (1994).
5. G. T. Camacho and M. Ortiz, Int. J. Solids. Struct. **33**, 2899 (1996).

6. J. W. Hutchinson and A. G. Evans, Acta Mater. **48**, 125 (2000).
7. P. A. Klein, J. W. Foulk, E. P. Chen, S. A. Wimmer, and H. J. Gao, Theor. Appl. Fract. Mech. **37**, 99 (2001).
8. W. Xuan, W. A. Curtin, and A. Needleman, Engng. Frac. Mech. **70**, 1869 (2003).
9. V. Tvergaard and J. W. Hutchinson, J. Mech. Phys. Solids **40**, 1377 (1992).
10. V. Tvergaard and J. W. Hutchinson, J. Mech. Phys. Solids **44**, 789 (1996).
11. J. W. Foulk III, G. C. Johnsonb, P. A. Klein, and R. O. Ritchie, J. Mech. Phys. Solids **56**, 2381 (2008).
12. Q. D. Yang, M. D. Thouless, and S. M. Ward, J. Mech. Phys. Solids **47**, 1337 (1999).
13. Q. D. Yang, M. D. Thouless, and S. M. Ward, J. Adhesion **72**, 115 (2000).
14. Q. D. Yang and M. D. Thouless, Int. J. Frac. **110**, 175 (2001).
15. J. L. Chaboche, F. Feyel, and Y. Monerie, Int. J. Solids Struct. **38**, 3127 (2001).
16. Y. F. Gao and F. A. Bower, Modelling Simul. Mater. Sci. Eng. **12**, 453 (2004).
17. R. Lorefice, G. Etse, and I. Carol, Int. J. Solids And Struct. **45**, 2686 (2008).
18. D. H. Warner, F. Sansoz, and J. F. Molinari, Int. J. Plasticity **22**, 754 (2006).
19. Y. J. Wei and L. Anand, J. Mech. Phys. Solids **52**, 2587 (2004).
20. C. Su, Y. J. Wei, and L. Anand, Int. J. Plasticity. **20**, 2063 (2004).
21. Y. J. Wei and L. Anand, Int. J. Solids Struct. **45**, 2785 (2008).
22. A. A. Volinsky, N. R. Moody, and W. W. Gerberich, Acta Mater. **50**, 441 (2002).
23. S. Kamiya, H. Kimura, K. Yamanobe, M. Saka, and H. Abe, Thin Solid Films **414**, 91 (2002).
24. B. A. Bibly, A. H. Cottrell, and K. H. Swinden, Proc. Roy. Soc. Lond. **A272**, 304 (1963).
25. G. Bao and Z. Suo, Appl. Mech. Rev. **45**, 355 (1992).
26. Abaqus FEA: Dassault Systmes Simulia Corp (2008).
27. G. Irwin, J. Appl. Mech. **24**, 361 (1957).
28. L. Y. Jiang, Y. G. Huang, H. Jiang, G. Ravichandran, H. Gao, K.C. Hwang, and B. Liu, J. Mech. Phys. Solids **54**, 2436 (2006).
29. W. B. Lu, J. Wu, L. Y. Jiang, Y. Huang, K. C. Hwang, and B. Liu, Phil. Mag. **87**, 2221 (2007).